The dynamic ocean redox evolution during the late Cambrian SPICE: Evidence from the I/Ca proxy

Ruliang He, Alexandre Pohl, Ashley Prow, Ganqing Jiang, Chin Chai Huan, Matthew Saltzman, Zunli Lu

The dynamic ocean redox evolution during the late Cambrian SPICE: evidence from the I/Ca proxy

Ruliang He[1,2*], Alexandre Pohl[3], Ashley Prow[2], Ganqing Jiang[4], Chin Chai Huan[4], Matthew R. Saltzman[5], Zunli Lu[2*]

[1] State Key Laboratory of Continental Dynamics, Shaanxi Key Laboratory of Early Life and Environments, Department of Geology, Northwest University, Xian 710069, People's Republic of China

[2] Department of Earth and Environmental Sciences, Syracuse University, Syracuse, NY 13244, United States

[3] Biogéosciences, UMR 6282 CNRS, Université de Bourgogne, 6 boulevard Gabriel, 21 000 Dijon, France

[4] Department of Geoscience, University of Nevada, Las Vegas, NV 89154, United States

[5] School of Earth Sciences, The Ohio State University, Columbus, OH 43210, United States

* Corresponding authors: rulianghe@nwu.edu.cn (Ruliang He), zunlilu@syr.edu (Zunli Lu)

Abstract

The late Cambrian Steptoean positive carbon isotope excursion (SPICE) is a distinct chemostratigraphic feature of the Paleozoic, marked by a 4–5‰ shift in carbonate $\delta^{13}C$ that has been recognized across the globe during the Paibian Stage. The SPICE may be related to enhanced burial of organic matter and pyrite during the expansion of marine euxinia, which as a source of O_2 also results in a pulse of atmospheric oxygen. However, geochemical proxies have not clearly illustrated how the ocean redox evolved with atmospheric oxygen changes during SPICE. This study presents new carbonate I/Ca data, a redox proxy for the upper ocean, from three basins. I/Ca values are low at Great Basin and South China from early into the peak of SPICE, indicating generally anoxic conditions in shallow waters. The overall increasing trend in I/Ca through the peak and recovery phase of the SPICE roughly correlates with the previously modeled rise in atmospheric oxygen. Spatially, the Georgina Basin (Mt. Whelan) might have recorded a relatively more oxic upper ocean compared to the Great Basin and South China. Earth system model

simulations also demonstrate the importance of paleogeographic and oceanographic settings on local redox conditions, highlighting the redox heterogeneity during SPICE.

Keywords: I/Ca, redox condition, late Cambrian, SPICE, Earth system model

1. Introduction

The Cambrian carbonate successions host several distinct carbon isotope ($\delta^{13}C$) excursions that often coincide with important extinctions and evolutionary radiations (Peng et al., 2020; Zhu et al., 2006). One of the most prominent $\delta^{13}C$ excursions happened during the Paibian Stage (~497–494 Ma) of the Furongian Series, referred to as the Steptoean positive carbon isotope excursion (SPICE), which has been recognized globally and represents a profound perturbation of the carbon cycle (Ahlberg et al., 2009; Brasier, 1993; Glumac and Walker, 1998; Pulsipher et al., 2021; Saltzman et al., 2004; Saltzman et al., 2000; Saltzman et al., 1998; Zhu et al., 2004). The onset of the SPICE is closely related to the first appearance of the cosmopolitan agnostoid trilobite *Glyptagnostus reticulatus* at the base of the Paibian Stage (Peng et al., 2009; Saltzman et al., 1998; Zhu et al., 2006). It also coincides with the turnover of the Marjumiid-Pterocephaliid biomere (a biostratigraphic interval that is bounded by sharp extinction events) in Laurentia (Palmer, 1984) and coeval extinction horizons in Gondwana and other continents (Peng, 1992; Saltzman et al., 2000; Saltzman et al., 1998). More broadly, the SPICE is thought to have fueled the explosion of phytoplankton diversity and modified the trophic structure with a long-term impact on the Great Ordovician Biodiversification Event (GOBE) (Saltzman et al., 2011; Servais et al., 2016). Elucidating the trend of ocean redox evolution during the SPICE is thus essential for understanding its relationship with late Cambrian biotic turnovers (Palmer, 1984) and early-middle Ordovician biodiversification.

1.1 The ocean redox during the SPICE

An increased burial of organic matter and pyrite during the SPICE, a major source for atmospheric oxygen, should lead to a rise in the atmospheric pO_2 (Saltzman et al., 2011). However, this atmospheric oxygenation event has not been clearly captured by marine redox proxies. Globally parallel positive excursions of carbonate-associated sulfur (CAS) and carbon isotopes in carbonate rocks suggest a widespread expansion of ocean euxinia during the peak of the SPICE (Gill et al., 2011; Hurtgen et al., 2009; Zhang et al., 2022). The U and Mo isotopes from carbonate and shales and Mo/TOC in euxinic shales also support an increase of anoxic seafloor area and a drawdown

of trace element inventory as euxinic conditions expanded (Dahl et al., 2014; Gill et al., 2021; Gill et al., 2011; Zhao et al., 2023). Many other redox proxy data, such as the enrichment of trace metals, highly reactive iron and glauconite, further demonstrate that local anoxic conditions happened at different stages of the SPICE across the continents (Gill et al., 2011; LeRoy and Gill, 2019; LeRoy et al., 2021; Mackey and Stewart, 2019; Pruss et al., 2019).

The widely distributed carbonate facies have the potential for a better reconstruction of shallow ocean redox conditions across the SPICE (e.g., Gill et al., 2011; Pulsipher et al., 2021; Saltzman et al., 2000). More importantly, considering the close contact with the atmosphere, the shallow ocean should be most sensitive to the oxygenation; and therefore, as an upper ocean redox proxy, the I/Ca ratio is suitable for investigating the influences of pO_2 rise on the shallow ocean during the late Cambrian.

1.2 The I/Ca redox proxy

Iodine is a biophilic, redox sensitive element in seawater (Elderfield and Truesdale, 1980; Küpper et al., 2011; Luther and Campbell, 1991). In the modern ocean, iodine has a global mean residence time of >300 kyr and a uniform surface concentration of ~0.45 μmol/L (Broecker and Peng, 1982; Chance et al., 2014). Iodate, IO_3^-, is the thermodynamically stable form of iodine at oxic conditions, whereas iodide, I^-, is the dominant form at depth in anoxic water and pore fluids (Luther and Campbell, 1991). In carbonates formed under oxic conditions, IO_3^- is incorporated into the crystal lattice by substituting CO_3^{2-}, while under low oxygen conditions the predominant iodide form is excluded (Feng and Redfern, 2018; Lu et al., 2010). The ratio of I/Ca in carbonates thus reflects local water column redox state (e.g., Zhou et al., 2015). Relatively high I/Ca values in bulk carbonate imply precipitation under oxic conditions, whereas lower values are indicative of deposition under oxygen depleted conditions (Lu et al., 2010). Lithologic variation does not exert considerable control on bulk I/Ca ratios; however it is recommended that detailed carbonate lithology is reported alongside I/Ca ratios (He et al., 2022). Furthermore, diagenetic alteration, usually influenced by iodate-depleted meteoric or anoxic pore water, is expected to only reduce I/Ca values (Hardisty et al., 2017; Lau and Hardisty, 2022).

In this study, we report new I/Ca data spanning the whole SPICE interval, from six sites of multiple depositional depths and basins, including Great Basin (USA), South China, and Georgina Basin (Australia). The ocean redox evolution trend across the SPICE is reconstructed and the impact of

atmospheric oxygenation and euxinia expansion is discussed. Lastly, using Earth System model simulations, we discuss the paleogeographic and oceanographic controls on the spatial patterns of ocean redox condition across multiple basins during SPICE.

2. Samples and methods

2.1 Geological background and samples

2.1.1 Great Basin, United States

During the late Cambrian, the northern edge of Laurentia was a subsiding passive margin of the Panthalassic Ocean (Fig. 1) (Mount and Bergk, 1998; Rees, 1986). The Great Basin of the western coterminous United States was situated equatorially during the Furongian (Fig. 1) (Osleger and Read, 1991; Palmer, 1960; Palmer and Holland, 1971). Late Cambrian strata are exposed on a NE-SW transect across most of Nevada, Western Utah and Wyoming and southern Montana and Idaho (Mount and Bergk, 1998). In North America, the Pterocephaliid biomere is equivalent to the Steptoean stage (Ludvigsen and Westrop, 1985). The Great Basin is an extensively studied region and the only North American depocenter that continuously yields Pterocephaliid trilobites for biostratigraphic correlation (Palmer, 1984). In the Great Basin the SPICE starts in the *Aphelaspis* trilobite zone, peaks in the late Steptoean *Dunderbergia* zone, corresponding to the Sauk II-Sauk III sequence boundary and major change in sedimentation regime, and returns to pre-excursion values in the *Elvina* zone (Glumac and Mutti, 2007; Saltzman et al., 1998).

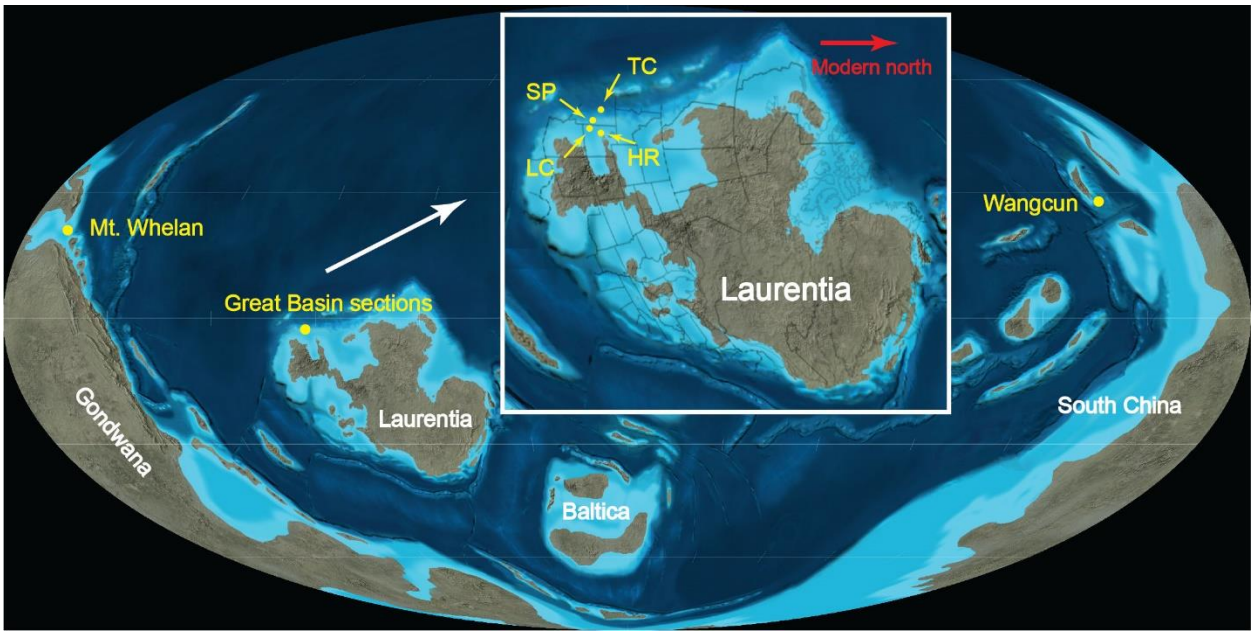

Fig. 1 The paleogeographic map of late Cambrian (~500 Ma) showing sampling locations of this study (Blakey, 2018), including Great Basin sections of North America, Mt. Whelan of Australia and Wangcun of South China. The inset shows locations of Shingle Pass (SP), House Range (HR), Lawson Cove (LC), Tybo Canyon (TC) in Great Basin.

House Range

The Little Horse Canyon exposure in the northern House Range, Utah represents deposition in a transiently restricted basin on a shallow carbonate platform (Rees, 1986; Saltzman et al., 1998). Here the Pterocephaliid biomere of the Orr Formation consists of, in ascending order, the Candland Shale, Johns Wash Limestone, Corset Spring Shale, and Sneakover Limestone members. The Orr Formation is overlain by the latest Cambrian-earliest Ordovician Notch Peak Formation (Miller et al., 2012; Osleger and Read, 1991). The sharp contact between the underlying Big Horse Limestone Member of the Orr Formation and the Candland Shale – the most fossiliferous unit – indicates an abrupt transition from peritidal to subtidal deposition (Hintze and Palmer, 1976; Widiarti, 2011; Zeiza, 2010). The Candland Shale is composed of interbedded fissile shale and dark grey, thinly bedded limestone (Hintze and Palmer, 1976). The upward shallowing into a dark grey oolitic limestone of the lower Johns Wash Limestone, followed by interbedded shale and limestone of the Corset Spring Shale, is interpreted to be progradation and retrogradation of a lagoonal - shoal system (Saltzman et al., 1998). The overlying Sneakover Limestone transitions from peritidal facies to wackestone and lime mudstones representing rapid transition to deeper deposition on an open shelf (Gill et al., 2011). The SPICE in this section spans three Pterocephalid biozones, *Aphelaphis, Dunderbergia,* and *Elvina* (Hintze and Palmer, 1976).

Lawson Cove

At the Lawson Cove section, southwest of the House Range in modern geography (Fig. 1), the Orr Formation comprises the lower Steamboat Pass Member and upper Sneakover Member. The meter-scale cyclic succession of the Steamboat Member represents episodic shallowing from lagoonal conditions (algal boundstones, peloidal packstones) to deeper intrashelf setting (burrowed wackestone) before returning to shallow facies of the lower Sneakover Member (Gill et al., 2011). Burrowed wackestone and trilobite packstones in the Steamboat Pass Member are inferred to have deposited under partly oxygenated conditions (Saltzman et al., 1998).

Shingle Pass

The late Cambrian strata at the Shingle Pass in the Egan Range, Nevada includes the Emigrant Springs Limestone, Dunderberg Formation and Whipple Cave Formation (Kellogg, 1963). The Emigrant Springs Limestone is divided into three members, A, B, and C. The Pterocephaliid biomere (and thus the SPICE) are present in Member C of Emigrant Springs Limestone and Dunderberg Formation (Kellogg, 1963). In later studies, Member C of the Emigrant Springs Limestone and Dunderberg Formation are correlated to or renamed as the Johns Wash Limestone and Corset Spring Shale, respectively (e.g., Saltzman et al., 1998; Gill et al., 2011). The Emigrant Springs Member C (or Johns Wash Limestone) is dominated by massive beds of oolitic/bioclastic grainstone, with wackestone and packstone interbeds, which have been interpreted as deposition from a shallow open marine shoal complex (Gill et al., 2011; Kellogg, 1963; Zeiza, 2010). The Dundenburg Shale (or Corset Spring Shale) in this section is composed of bioclastic wackestone and packstone, with grainstone, lime mudstone, and shale interbeds, which were likely deposited from shallow-deep subtidal environments (Gill et al., 2011; Kellogg, 1963; Saltzman et al., 1998; Zeiza, 2010). The overlying Whipple Cave Formation consists of mainly cherty limestone and dolostone with abundant stromatolites and thrombolites that were interpreted as deposition from a shelf margin shoal complex (Cook and Taylor, 1975; Kellogg, 1963).

Tybo Canyon

Tybo Canyon is located west of Shingle Pass in the Hot Creek Range, Nevada (in modern geography, Fig. 1). The late Cambrian strata in this section includes the Swarbrick Limestone, Dunderberg Shale, and the lower part of the Hales Limestone (Cook and Corboy, 2004). The Swarbrick Limestone consists of gray, thinly laminated lime mudstone characteristic of marginal slope facies. The Dunderberg Shale is composed of olive grey shale, siltstone and lime mudstone that were deposited from slope-basin environments (Kellogg, 1963; Taufani, 2012; Taylor et al., 1991). The Hales Limestone consists of lime mudstone and wackestone, with abundant debris-flow breccias and turbidities, which were interpreted as submarine fan deposits (Cook and Corboy, 2004; Cook and Taylor, 1975; Taufani, 2012). The SPICE in this section occurs in the upper part of the Dunderberg Shale and the lowermost Hales Limestone.

2.1.2 Mount Whelan, Queensland, Australia

The sedimentary succession in the Mt. Whelan core was deposited in the late Cambrian to Lower Ordovician Georgina basin (Fig. 1) (Lam and Mckillop, 2009). The continuous Georgina Limestone spans the entire Paibian stage and consists of millimeter scale laminated argillaceous micrite with calcite and pyrite nodules distributed throughout (Gill et al., 2011; Saltzman et al., 1998). The depositional environment is inferred to be deep subtidal (below wave base) throughout. The C, S and U isotope data have been reported in other publications (Dahl et al., 2014; Gill et al., 2011; Saltzman et al., 2000).

2.1.3 Wangcun, South China

The Wangcun section in South China is on the Jiangnan Slope Belt, which represents a transitionary complex separating the shallow water carbonates of the Yangtze Platform and the deep basinal deposits of the Jiangnan Basin in South China, which is located on the northwestern margin of Gondwana continent (Fig. 1) (Saltzman et al., 2011; Zhu et al., 2004; Zuo et al., 2018). The Huaqiao Formation encompasses the entire Paibian stage at the Wangcun section, Hunan Province (Peng et al., 2004; Zuo et al., 2018). Our samples are from the lower member of the Huaqiao Formation, which consists of rhythmic argillaceous limestones and calcareous shales, with minor interbeds of dolomitic limestone (Saltzman et al., 2011). Carbonate carbon isotope data have been previously reported by Saltzman et al. (2011).

2.2 I/Ca measurement

A total of 170 new I/Ca measurements were taken from Shingle Pass (n = 56), the House Range (n = 54) and Tybo Canyon (n = 60) in the Great Basin. Approximately 2–4 mg of powdered samples were accurately weighed and rinsed with deionized water to remove surface bound iodine. The carbonate fraction was dissolved in 3% nitric acid and the supernatant containing the carbonate associated iodate was pipetted into a clean vial. The supernatant was diluted with matrix-matching solution to ~50 ppm Ca depending on initial sample mass. The matrix solution was prepared with 5 pbb indium and cesium internal standards and buffered with 0.5% tertiary amine, which stabilizes the iodine. To avoid loss of iodine by volatilization, samples were immediately analyzed by inductively coupled plasma mass spectrometry (ICP-MS Bruker M90) at Syracuse University. Calibration solutions and reference standards were prepared fresh before analysis. Instrument sensitivity was tuned to 80–100k counts per second for a 1 ppb iodine standard and long-term

accuracy was ensured by routine measurements of JCp-1 standard (Lu et al., 2020b). Detailed sample preparation and instrumental analysis of I/Ca in carbonates is outlined in Lu et al. (2020b).

2.3 Chemostratigraphic correlation

The carbon isotope chemostratigraphy is important for Cambrian stratigraphic correlation because of the lack of index fossils for key horizons in some locations (Peng et al., 2020). Saltzman et al. (1998) provide the basis for $\delta^{13}C$ chemostratigraphic correlation in the Great Basin allowing more precise recognition of the SPICE in variable carbonate facies. Therefore, the correlation for the six sites in this study is adopted from Saltzman et al. (1998). The six sections (or cores) were first divided into eight isotope stages by 1‰ divisions of the SPICE excursion for section correlation. They were all then correlated to the Shingle Pass section because it has a relatively high depositional rate and a continuous carbon isotope record. Lastly, for simplification, the discussion only focuses on three major phases of the SPICE, including the rising limb (< 2‰), peak of SPICE (> 2‰), and the falling limb (< 2‰) (Fig. 2).

2.4 Earth System Model experiments

2.4.1 Description of the model

cGENIE is an Earth System Model of intermediate complexity that allows for spatial visualization of possible circulation scenarios and chemical tracer distributions (Ridgwell et al., 2007). It consists of a three-dimensional frictional geostrophic, biogeochemistry-enabled ocean circulation model coupled to a 2D energy-moisture-balance atmospheric component and a sea-ice model. We configured the model on a 36×36 equal-area grid with 17 unevenly spaced vertical levels to a maximum depth of ca. 5900 m in the ocean. The cycling of carbon and associated tracers in the ocean is based on a single (phosphate) nutrient limitation of biological productivity (Stockey et al., 2021), but adopts the Arrhenius-type temperature-dependent scheme for the remineralization of organic matter exported to the ocean interior (Crichton et al., 2021). Despite its low spatial resolution, cGENIE satisfactorily simulates ocean [O_2] spatial patterns and values in the modern (Ridgwell et al., 2007) and deep past (Pohl et al., 2021).

2.4.2 Description of the numerical experiments

We configured cGENIE to represent plausible Cambrian environmental conditions, using a paleogeographical reconstruction for 500 Ma (Scotese and Wright, 2018), lowered solar

luminosity (1312 W m^{-2}) (Gough, 1981) and increased atmospheric partial pressure of CO_2 (~4350 ppm, or equivalently close to 16 times the preindustrial concentration) (Krause et al., 2018). We employed a null eccentricity-minimum obliquity orbital configuration, which provides an equal mean annual insolation to both hemispheres with minimum seasonal contrasts. The ocean nutrient inventory was kept to Modern (2.1 μmol kg^{-1} PO_4). We varied the atmospheric partial pressure of oxygen (pO_2) to quantify the impact of atmospheric oxygenation on upper-ocean dissolved oxygen concentrations ($[O_2]$). In detail, we conducted 2 experiments tentatively representative of pre-SPICE and post-SPICE conditions, characterized by atmospheric pO_2 levels of respectively ×0.6 Modern (12.5%) and ×1.2 Modern (25%). These estimates are derived from the carbon cycle modeling of Saltzman et al. (2011), although we acknowledge that alternative models for the drivers of large positive CIEs continue to be explored in the literature (e.g., Geyman and Maloof, 2019; Higgins et al., 2018).

To generate the physical atmospheric boundary conditions required by cGENIE for this new 500 Ma continental configuration, we ran a 100-year simulation under identical boundary conditions with the slab mixed-layer ocean model FOAM. We then derived the 2D wind speed and wind stress, and 1D zonally-averaged albedo forcing fields required by the cGENIE model, using the 'muffingen' open-source software (DOI: 10.5281/zenodo.5500687), following the methods employed in Pohl et al. (2022).

cGENIE simulations were initialized with a sea-ice free ocean and homogeneous temperature and salinity in the ocean (5°C and 33.9‰, respectively) and integrated for a total of 20,000 years. Results of the last simulated year were analyzed.

3. Results

3.1 Carbon isotope

The $\delta^{13}C_{carb}$ values were measured in three Great Basin sections (Shingle Pass, House Range, Tybo Canyon) showing similar stratigraphic trends (Baker, 2010; Taufani, 2012). The background of late Cambrian $\delta^{13}C_{carb}$ is in the range of ~ 0–1 ‰, while the abrupt positive excursions up to ~5 ‰ are observed for all the sites, indicating that the SPICE is fully captured (Fig. 2). The Lawson Cove section and Mt. Whelan core, two previously published datasets, also have similar carbon isotope trends. The Wangcun section does not capture the falling limb of SPICE in Paibian Stage (Fig. 2),

while its $\delta^{13}C_{carb}$ profile is comparable to the Wa'ergang and Paibi sections in South China (Saltzman et al., 2000).

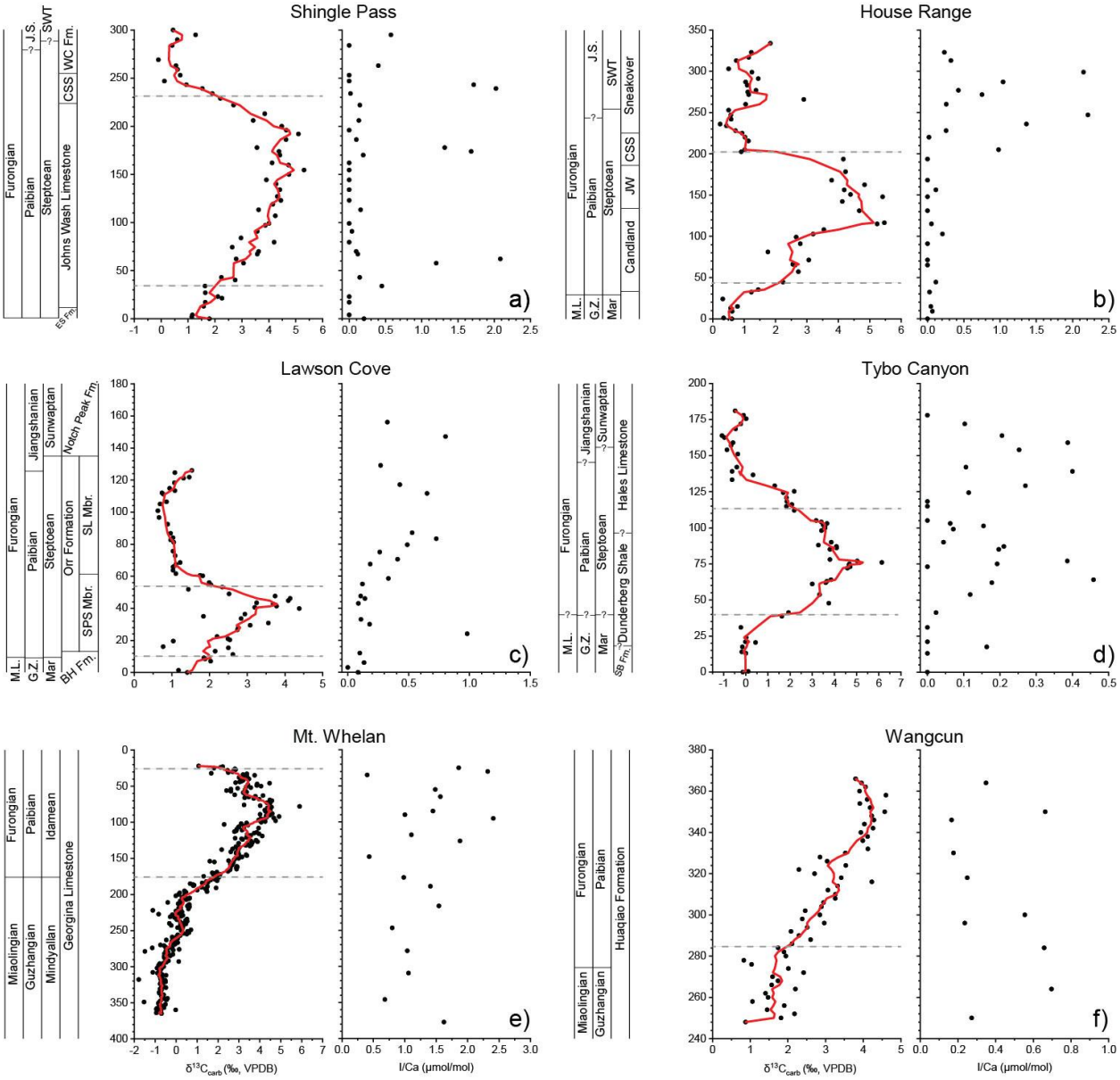

Fig. 2 Stratigraphic $\delta^{13}C$ and I/Ca data for a) Shingle Pass, b) House Range, c) Lawson Cove, d) Tybo Canyon, e) Mt. Whelan and f) Wangcun of South China. The red lines show running averages of $\delta^{13}C$ for each site. The peak of SPICE is defined by the interval with $\delta^{13}C > 2‰$, and the grey dashed lines show the boundaries. Note the falling limb is not observed in the Wangcun section. Abbreviations: M.L. = Miaolingian, G.Z. = Guzhangian, J.S. = Jiangshanian, Mar = Marjuman,

SWT= Sunwaptan, ES = Emigrant Springs, CSS = Corset Spring Shale, WC = Whipple Cave, JW = Johns Wash, SPS = Steamboat Pass Shale, SL = Sneakover Limestone, SB = Swarbrick.

3.2 I/Ca ratio

The House Range and Lawson Cove sections have a low I/Ca background (near detection limit) in the rising limb and peak of SPICE; the I/Ca ratios show an increase up to 2 µmol/mol at the falling limb and the post-SPICE interval (Figs. 2b and c). The more distal Shingle Pass and Tybo Canyon show a less prominent rise of I/Ca and have generally low I/Ca (< 0.5 µmol/mol) across the sections, with pulses of I/Ca (up to 2 µmol/mol) being occasionally found in Shingle Pass (Figs. 2a and d). Overall, the composite section of the Great Basin (Fig. 3) shows an I/Ca increase up to 3 µmol/mol at the recovery phase of SPICE (Figs. 3c, d). In the Georgina Basin of Australia, the Mt. Whelan core has a higher I/Ca background than the Great Basin with most values in the range of 2 to 3 µmol/mol (Fig. 2e). It shows an increase of I/Ca from pre- to peak of SPICE, except for a dip at ~150 m (Figs. 3h, i). The mean I/Ca ratio increases from 1.03 to 1.52 µmol/mol from pre- to peak of SPICE (Fig. 3i), and the nonparametric Mann-Whitney Test show a p-value of 0.06. The Wangcun section from South China contains low I/Ca values (< 1 µmol/mol) (Fig. 2f).

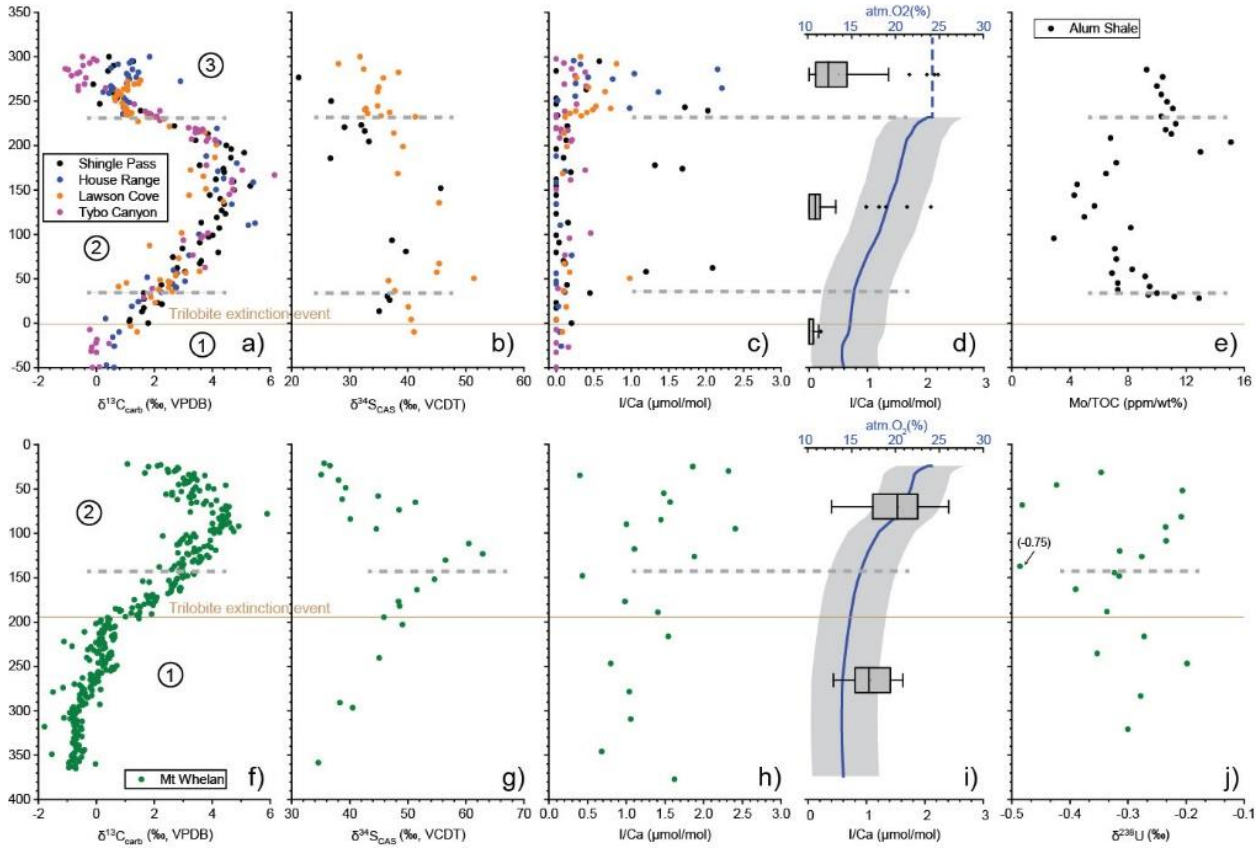

Fig. 3 Stratigraphic I/Ca data and geochemical data compilation for Great Basin sections (a–e) and for the Mt. Whelan core (f–j). Great Basin sections are plotted by adjusting stratigraphic heights after section correlation: a) $\delta^{13}C_{carb}$, b) $\delta^{34}S_{CAS}$, c) I/Ca ratio, d) I/Ca box plots for each SPICE stage and modeled pO_2 (Saltzman et al., 2011), e) Mo/TOC of Alum Shale of Baltica (Gill et al., 2011). The Mt. Whelan core: f) $\delta^{13}C_{carb}$, g) $\delta^{34}S_{CAS}$, h) I/Ca ratio, i) I/Ca box plots for each SPICE stage and modeled pO_2 (Saltzman et al., 2011), j) carbonate U isotope (Dahl et al., 2014). The dashed blue line in d) represents a stable state after the pulse of pO_2 (Saltzman et al., 2011); the pO_2 curves are normalized to stratigraphic height/depth of Shingle Pass and Mt. Whelan in panel d) and i) respectively. The dashed grey lines divide the Great Basin into three phases and the Mt. Whelan core into two phases: 1 = pre- and early SPICE, 2 = peak of SPICE, 3 = late SPICE.

4. Discussion

4.1 The atmospheric oxygenation and its impact on I/Ca signal

Major atmospheric oxygen rises are likely to impact the shallow water redox state directly because of the important gas transfers with the overlying atmosphere. Such conditions have been recorded by higher I/Ca ratios, for example, during the great oxidation event (GOE) and Devonian oxygenation (Hardisty et al., 2014; He et al., 2020). However, these studies at low temporal resolution were unable to capture how the subsurface redox conditions evolved relative to the atmosphere and deep ocean. The SPICE presents such an opportunity. The mass balance model, based on positive C and S isotope excursions, suggests that an increased pO_2 level, with a net O_2 production up to 19×10^{18} moles or 10% O_2, accompanied the development of SPICE due to increased burial of organic matter and pyrite (Saltzman et al., 2011). The pO_2 rise starts gradually with the initiation of SPICE, and increases sharply in a 2-Myr period during the peak of SPICE related to the peak of organic carbon and pyrite burial (Saltzman et al., 2011). After the SPICE, although C and S isotopes fall to their pre-excursion values, the mass balance model suggests a continued impact on the ocean redox states (Saltzman et al., 2011). Our I/Ca data support the modeled atmospheric oxygenation. The Mt. Whelan core shows an increase of I/Ca at early SPICE, and the I/Ca ratios of Great Basin sections increase to a level greater than the background of pre-SPICE during the recovering phase of $\delta^{13}C$ excursion (Figs. 3d, i).

Other redox proxies, such as U, Mo isotopes and Mo/TOC (Fig. 3) which are sensitive to the euxinic burial of U and Mo on the seafloor, did not seem to be significantly impacted by

atmospheric conditions, and never evolved to a more oxygenated state relative to the pre-excursion level (Dahl et al., 2014; Gill et al., 2021; Gill et al., 2011; Zhao et al., 2023). The bottom water changes may have lagged behind the shallow water. Alternatively, deeper parts of global oceans were not significantly impacted by the pO_2 rise, as Earth system models suggest that upper- and deep-ocean oxygen concentrations may have been decoupled during the early Paleozoic (Pohl et al., 2021; Pohl et al., 2022).

4.2 Local redox variations in Great Basin

The four sections of the Great Basin represent a gradient of depositional depth from carbonate shelf to slope, providing a transect to delineate the tempo-spatial redox pattern for different stages of SPICE (Fig. 4).

Pre- and early-SPICE

Frequent ocean anoxia likely dominated the Early Paleozoic until the late Silurian to Devonian (Dahl et al., 2010; Elrick et al., 2022; He et al., 2020; Krause et al., 2018; Sperling et al., 2015; Tostevin and Mills, 2020; Wallace et al., 2017). During the pre-SPICE stage, an overall low I/Ca background (< 0.5 μmol/mol) is found in the Great Basin (Figs. 2, 3). In the modern ocean, such low I/Ca values are usually seen in planktonic foraminifera shells near the oxygen minimum zones (OMZs), related to very low concentrations of iodate (IO_3^-) and thus a generally oxygen-depleted condition in the upper ocean (Lu et al., 2020a; Lu et al., 2016). Although a direct comparison of I/Ca measurements in ancient rocks vs. in Cenozoic foraminifera has its own challenges, the I/Ca data likely suggest the anoxic condition (or a shallow oxycline) may had been pervasive across continental shelves of Eastern Laurentia during the pre- and early-SPICE interval (Fig. 4a).

Peak of SPICE

During the peak of SPICE, the I/Ca range is still characterized by a very low background (< 0.5 μmol/mol; Fig. 3c), suggesting a continuation of the already anoxic background of the pre-SPICE interval. At the same time, increased burial of organic matter and pyrite and a depleted trace metal inventory suggest a widespread expansion of euxinic conditions from deep basin to shallow shelves (Gill et al., 2011) (Fig. 4b). The I/Ca proxy itself is not expected to the transition from anoxic to euxinic conditions, since iodate reduction should be complete immediately after dissolved oxygen is exhausted (Fig. 4b).

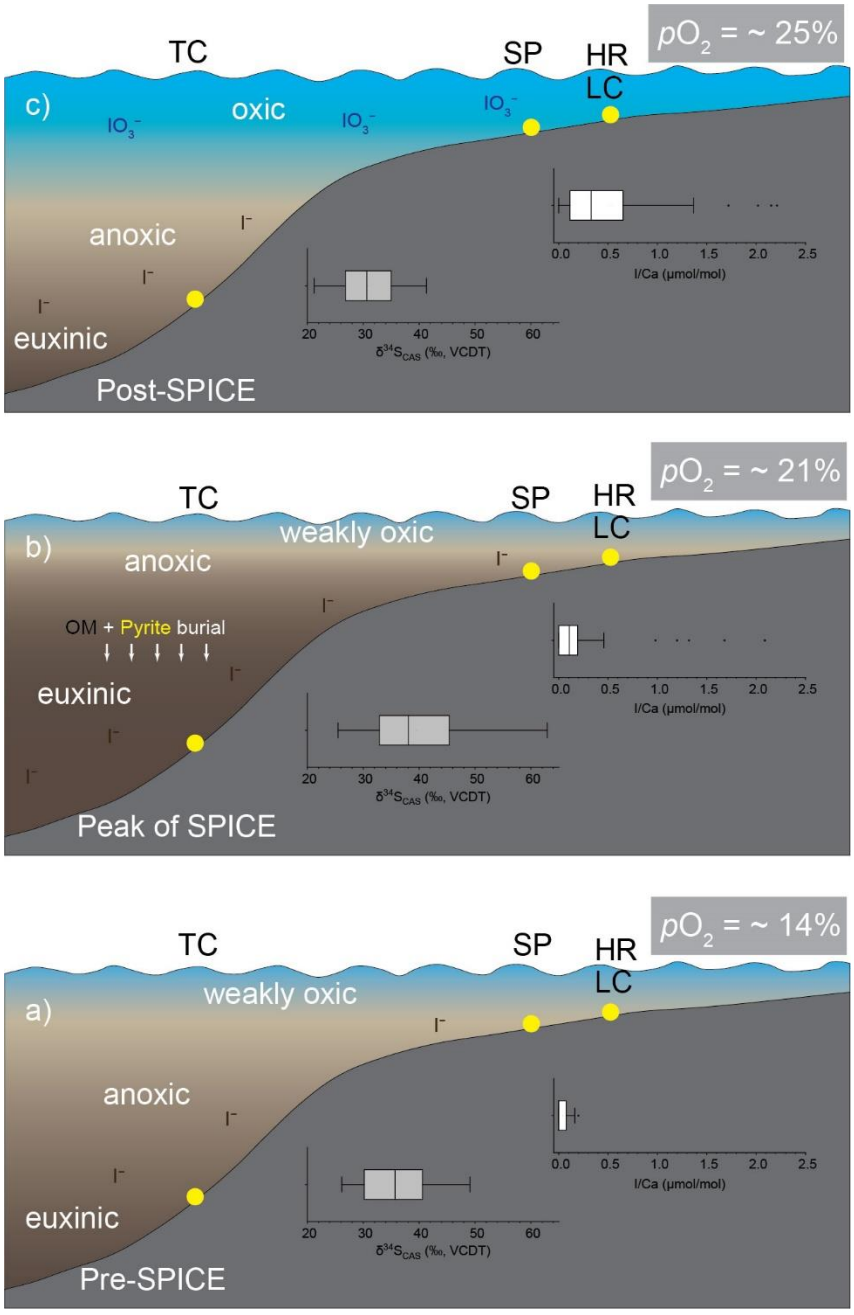

335

336 **Fig. 4** A conceptual model for ocean redox condition during late Cambrian SPICE: a) an overall
337 anoxic condition during the pre-SPICE stage; b) an expansion of euxinic conditions with enhanced
338 burial of organic carbon and pyrite during the peak of SPICE; c) a well-oxygenated shallow
339 subsurface with anoxic deeper water during post-SPICE stage. The box plots in each panel are
340 I/Ca ratios of Great Basin sections (Shingle Pass, House Range, Lawson Cove, Tybo Canyon) of
341 this study and carbonate associated sulfate isotope data (Shingle Pass, Lawson Cove, TE-1 core,

Mt. Whelan core) from Gill et al. (2011). Abbreviations: SP = Shingle Pass, HR = House Range, LC = Lawson Cove, TC = Tybo Canyon, OM = organic matter.

Late-SPICE

Under the influence of atmospheric oxygenation during the Late-SPICE (Saltzman et al., 2011), the redoxcline might have be pushed deeper, resulting in more oxygenated upper ocean. Consequently, the shallower-water sections on the carbonate platform, such as House Range and Lawson Cove, all show increased I/Ca ratios in this interval. On the other hand, the deeper-water section on the shelf margin to slope environment, Tybo Canyon appeared to remain below the redoxcline (Fig. 4c). The Shingle Pass section, which possibly is on a more distal outer shelf environment relative to Lawson Cove and the House Range, only records sporadic occurrences of high I/Ca (Fig. 2). Alternatively, the relatively low I/Ca ratios found in Shingle Pass and Tybo Canyon sections may be related to the diagenetic process which usually decreases carbonate iodine contents and thereby lower original I/Ca ratios (Hardisty et al., 2017; Lau and Hardisty, 2022).

4.3 Simulated oceanic [O_2] in response to the SPICE redox dynamics

The pre-SPICE background

In our experiment representing pre-SPICE conditions (pO_2 of 12.5 %, see Methods), the Great Basin (both shallow and deep) and South China are all characterized by anoxic conditions, averaging at 0.34 μmol kg^{-1} [O_2], while oceanic [O_2] at Mt Whelan is significantly higher at 19.6 μmol kg^{-1} (Fig. 5b and blue points in Fig. 5c). Simulated [O_2] spatial patterns align well with pre-SPICE I/Ca data: all sites are poorly oxygenated except Mt. Whelan (Figs. 2, 5). From the perspective of paleogeography, during the late Cambrian the Great Basin and South China sections were all located along the western continental margins (Fig. 1). In the modern ocean, such region is usually influenced by upwelling and widely-developed OMZs like the Eastern Equatorial Pacific (EEP) and Namibia margin (Bograd et al., 2022; Chavez and Messié, 2009). Therefore, it is not surprising that the Mt. Whelan core might have been more oxygenated than other sections.

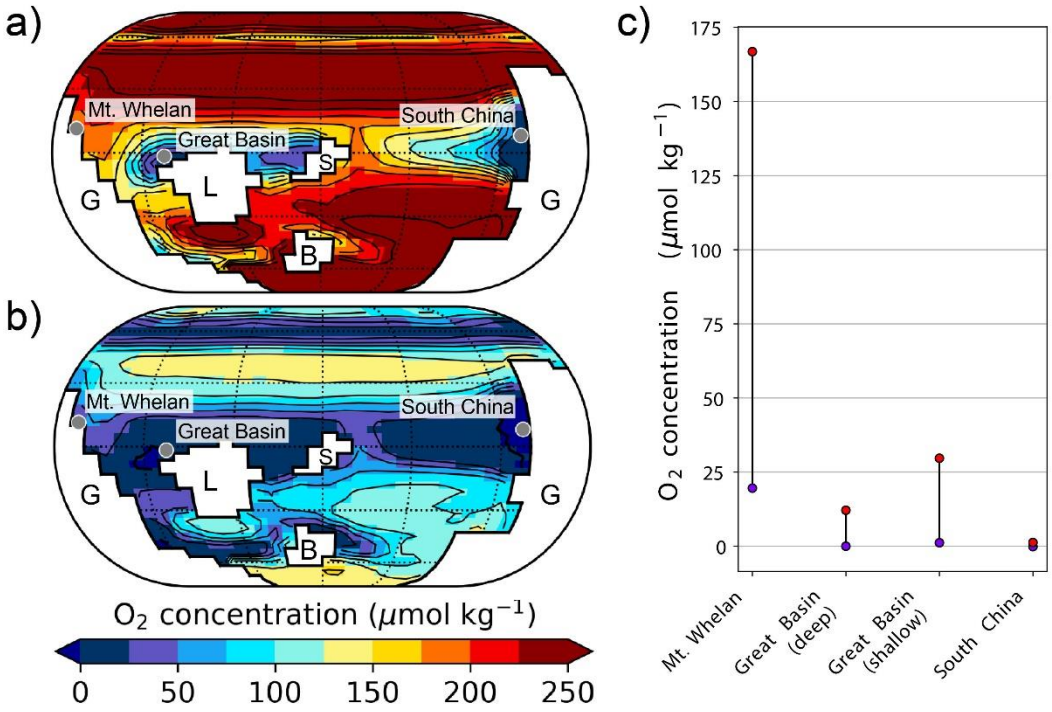

Fig. 5 Late Cambrian oceanic [O_2] simulated under different atmospheric pO_2 levels: a) Oceanic [O_2] at ~230 m water depth using a post-SPICE pO_2 of ×1.2 Modern, or equivalently 25 %; b) As per (a) using a pre-SPICE pO_2 of ×0.6 Modern (12.5 %); c) Change in oceanic [O_2] simulated in response to an increase of pO_2 from pre-SPICE levels of ×0.6 Modern (blue points) to post-SPICE levels of ×1.2 Modern (red points) at geological sampling locations discussed in the text at ~230 m water depth ('Mt. Whelan', 'Great Basin (deep)' and 'South China'). The same quantity is also given for the Great Basin at ~128 m water depth ('Great Basin (shallow)'). In panels (a) and (b), the projection is Eckert IV with parallels shown every 30° latitude. Landmasses are shaded white. G: Gondwana; L: Laurentia; B: Baltica; S: Siberia. Grey points represent the geological sampling locations discussed in the main text and used in panel (c).

The post-SPICE oxygenation

When atmospheric pO_2 is increased to 25% in the model – a perturbation supposedly representative of the changes in atmospheric composition during the SPICE – oceanic [O_2] concentrations show contrasting evolutions at the different sites of interest. In South China, there is virtually no change in oceanic [O_2] (Fig. 5a, b), which increases by only 1.4 μmol kg^{-1} (Fig. 5c). This is generally consistent with the low I/Ca values (< 0.8 μmol/mol) from the pre-SPICE interval to its peak (Fig. 2f), but more I/Ca data from the recovery phase of SPICE in South China are needed to validate

the results of cGENIE. On the other hand, the Great Basin displays a larger, concomitant increase in oceanic [O_2] at all the depths (Fig. 5c); and there are greater value rises to +28 μmol kg^{-1} in the shallower water column than the deeper one (+12 μmol kg^{-1}) at the same geographical location (Fig. 5c). Therefore, the model does simulate the larger oxygenation at shallower sites than at deeper sites in the Great Basin, in agreement with the larger I/Ca change at House Range and Lawson Cove than at Shingle Pass and Tybo Canyon.

The only clear mismatch between our numerical results and I/Ca proxy data is for Mt. Whelan, which shows a limited I/Ca increase but a very strong [O_2] change in cGENIE. At Mt Whelan, oceanic [O_2] increases by 147 μmol kg^{-1}. This discrepancy may reflect the limitations of our modeling setup, notably the poor representation of coastal environments on the coarse cGENIE model grid. We also cannot rule out the possibility that diagenesis suppressed the magnitude of increase in I/Ca associated with pO_2 rise.

5. Conclusion

Our new I/Ca data show a rise of I/Ca through the SPICE in different ocean basins. These data support the concept that the increased pO_2 levels impacted the upper ocean during SPICE. At Great Basin and South China, the shallow redoxcline associated with the burial of organic matter and pyrite during large portion of the SPICE appear to be a continuation from a pre-existing anoxic background of the late Cambrian. The Mt. Whelan of northeast Gondwana experienced less severe upper ocean deoxygenation during the SPICE. Earth system model simulations generally agree with the temporal trend and spatial pattern recorded by I/Ca proxy data, demonstrating an imprint of geographic and oceanographic conditions on the I/Ca signal of local redox.

Acknowledgement

This work was supported by NSF EAR-2121445 and OCE-1736542. This is a contribution of UMR 6282 Biogéosciences Team 'SEDS'. This is a contribution to UNESCO project IGCP 735 "Rocks and the Rise of Ordovician Life" (Rocks n' ROL). AP acknowledges the support of the French Agence Nationale de la Recherche (ANR) under reference ANR-22-CE01-0003 (project ECO-BOOST) and from CNRS INSU (project ROSETTA). The authors thank Dr. Andy Ridgwell for the help on the manuscript and uploading the files to GitHub.

Code availability

The code for the version of the 'muffin' release of the cGENIE Earth system model used in this paper, is tagged as v0.9.41, and is assigned a DOI: 10.5281/zenodo.7896760. Configuration files for the specific experiments presented in the paper can be found in the directory: genie-userconfigs/PUBS/submitted/He_etal.Gloplacha.2023. Details of the experiments, plus the command line needed to run each one, are given in the readme.txt file in that directory. All other configuration files and boundary conditions are provided as part of the code release. A manual detailing code installation, basic model configuration, tutorials covering various aspects of model configuration, experimental design, and output, plus the processing of results, is assigned a DOI: 10.5281/zenodo.7545814.

References

Ahlberg, P.E.R., Axheimer, N., Babcock, L.E., Eriksson, M.E., Schmitz, B., Terfelt, F., 2009. Cambrian high-resolution biostratigraphy and carbon isotope chemostratigraphy in Scania, Sweden: first record of the SPICE and DICE excursions in Scandinavia. Lethaia 42, 2-16.

Baker, J.L., 2010. Carbon isotopic fractionation across a late Cambrian carbonate platform: A regional response to the spice event as recorded in the Great Basin, United States, Geoscience. University of Nevada, Las Vegas, p. 116.

Blakey, R., 2018. Paleogeography and Geologic Evolution of North America. https://deeptimemaps.com/ (accessed at March 2018).

Bograd, S.J., Jacox, M.G., Hazen, E.L., Lovecchio, E., Montes, I., Pozo Buil, M., Shannon, L.J., Sydeman, W.J., Rykaczewski, R.R., 2022. Climate Change Impacts on Eastern Boundary Upwelling Systems. Ann Rev Mar Sci.

Brasier, M., 1993. Towards a carbon isotope stratigraphy of the Cambrian System: potential of the Great Basin succession. Geological Society, London, Special Publications 70, 341-350.

Broecker, W.S., Peng, T.-H., 1982. Tracers in the Sea. Lamont-Doherty Geological Observatory, Columbia University Palisades, New York.

Chance, R., Baker, A.R., Carpenter, L., Jickells, T.D., 2014. The distribution of iodide at the sea surface. Environ Sci Process Impacts 16, 1841-1859.
Chavez, F.P., Messié, M., 2009. A comparison of Eastern Boundary Upwelling Ecosystems. Progress in Oceanography 83, 80-96.
Cook, H.E., Corboy, J.J., 2004. Great Basin Paleozoic carbonate platform: Facies, facies transitions, depositional models, platform architecture, sequence stratigraphy, and predictive mineral host models. US Geological Survey Open-File Report 1078, 129.
Cook, H.E., Taylor, M.E., 1975. Early Paleozoic continental margin sedimentation, trilobite biofacies, and the thermocline, western United States. Geology 3, 559-562.
Crichton, K.A., Wilson, J.D., Ridgwell, A., Pearson, P.N., 2021. Calibration of temperature-dependent ocean microbial processes in the cGENIE.muffin (v0.9.13) Earth system model. Geoscientific Model Development 14, 125-149.
Dahl, T.W., Boyle, R.A., Canfield, D.E., Connelly, J.N., Gill, B.C., Lenton, T.M., Bizzarro, M., 2014. Uranium isotopes distinguish two geochemically distinct stages during the later Cambrian SPICE event. Earth Planet Sci Lett 401, 313-326.
Dahl, T.W., Hammarlund, E.U., Anbar, A.D., Bond, D.P., Gill, B.C., Gordon, G.W., Knoll, A.H., Nielsen, A.T., Schovsbo, N.H., Canfield, D.E., 2010. Devonian rise in atmospheric oxygen correlated to the radiations of terrestrial plants and large predatory fish. Proceedings of the National Academy of Sciences 107, 17911-17915.
Elderfield, H., Truesdale, V.W., 1980. On the biophilic nature of iodine in seawater. Earth and Planetary Science Letters 50, 105-114.
Elrick, M., Gilleaudeau, G.J., Romaniello, S.J., Algeo, T.J., Morford, J.L., Sabbatino, M., Goepfert, T.J., Cleal, C., Cascales-Miñana, B., Chernyavskiy, P., 2022. Major Early-Middle Devonian oceanic oxygenation linked to early land plant evolution detected using high-resolution U isotopes of marine limestones. Earth and Planetary Science Letters 581.
Feng, X., Redfern, S.A.T., 2018. Iodate in calcite, aragonite and vaterite CaCO3: Insights from first-principles calculations and implications for the I/Ca geochemical proxy. Geochimica et Cosmochimica Acta 236, 351-360.
Geyman, E.C., Maloof, A.C., 2019. A diurnal carbon engine explains (13)C-enriched carbonates without increasing the global production of oxygen. Proc Natl Acad Sci U S A 116, 24433-24439.
Gill, B.C., Dahl, T.W., Hammarlund, E.U., LeRoy, M.A., Gordon, G.W., Canfield, D.E., Anbar, A.D., Lyons, T.W., 2021. Redox dynamics of later Cambrian oceans. Palaeogeography, Palaeoclimatology, Palaeoecology 581.
Gill, B.C., Lyons, T.W., Young, S.A., Kump, L.R., Knoll, A.H., Saltzman, M.R., 2011. Geochemical evidence for widespread euxinia in the later Cambrian ocean. Nature 469, 80-83.
Glumac, B., Mutti, L.E., 2007. Late Cambrian (Steptoean) sedimentation and responses to sea-level change along the northeastern Laurentian margin: Insights from carbon isotope stratigraphy. Geological Society of America Bulletin 119, 623-636.
Glumac, B., Walker, K.R., 1998. A Late Cambrian positive carbon-isotope excursion in the Southern Appalachians; relation to biostratigraphy, sequence stratigraphy, environments of deposition, and diagenesis. Journal of Sedimentary Research 68, 1212-1222.
Gough, D., 1981. Solar interior structure and luminosity variations, Physics of Solar Variations: Proceedings of the 14th ESLAB Symposium held in Scheveningen, The Netherlands, 16–19 September, 1980. Springer, pp. 21-34.
Hardisty, D.S., Lu, Z., Bekker, A., Diamond, C.W., Gill, B.C., Jiang, G., Kah, L.C., Knoll, A.H., Loyd, S.J., Osburn, M.R., Planavsky, N.J., Wang, C., Zhou, X., Lyons, T.W., 2017. Perspectives

485 on Proterozoic surface ocean redox from iodine contents in ancient and recent carbonate. Earth
486 and Planetary Science Letters 463, 159-170.
487 Hardisty, D.S., Lu, Z., Planavsky, N.J., Bekker, A., Philippot, P., Zhou, X., Lyons, T.W., 2014.
488 An iodine record of Paleoproterozoic surface ocean oxygenation. Geology 42, 619-622.
489 He, R., Elrick, M., Day, J., Lu, W., Lu, Z., 2022. Devonian upper ocean redox trends across
490 Laurussia: Testing potential influences of marine carbonate lithology on bulk rock I/Ca signals.
491 Frontiers in Marine Science 9.
492 He, R., Lu, W., Junium, C.K., Ver Straeten, C.A., Lu, Z., 2020. Paleo-redox context of the Mid-
493 Devonian Appalachian Basin and its relevance to biocrises. Geochimica et Cosmochimica Acta
494 287, 328-340.
495 Higgins, J.A., Blättler, C.L., Lundstrom, E.A., Santiago-Ramos, D.P., Akhtar, A.A., Crüger Ahm,
496 A.S., Bialik, O., Holmden, C., Bradbury, H., Murray, S.T., Swart, P.K., 2018. Mineralogy, early
497 marine diagenesis, and the chemistry of shallow-water carbonate sediments. Geochimica et
498 Cosmochimica Acta 220, 512-534.
499 Hintze, L., Palmer, A., 1976. Upper Cambrian Orr Formation: its subdivisions and correlatives in
500 western Utah: United States Geological Survey Bulletin 1405-G.
501 Hurtgen, M.T., Pruss, S.B., Knoll, A.H., 2009. Evaluating the relationship between the carbon and
502 sulfur cycles in the later Cambrian ocean: An example from the Port au Port Group, western
503 Newfoundland, Canada. Earth and Planetary Science Letters 281, 288-297.
504 Kellogg, H.E., 1963. Paleozoic Stratigraphy of the Southern Egan Range, Nevada. GSA Bulletin
505 74, 685-708.
506 Krause, A.J., Mills, B.J., Zhang, S., Planavsky, N.J., Lenton, T.M., Poulton, S.W., 2018. Stepwise
507 oxygenation of the Paleozoic atmosphere. Nature communications 9, 4081.
508 Küpper, F.C., Feiters, M.C., Olofsson, B., Kaiho, T., Yanagida, S., Zimmermann, M.B., Carpenter,
509 L.J., Luther III, G.W., Lu, Z., Jonsson, M., 2011. Commemorating two centuries of iodine research:
510 an interdisciplinary overview of current research. Angewandte Chemie International Edition 50,
511 11598-11620.
512 Lam, J.S., Mckillop, M., 2009. A summary of company exploration results for minerals and
513 petroleum in the Mount Whelan 1:250 000 (SF54-13) Sheet area, central west Queensland.
514 Queensland Geological Record 2009/02.
515 Lau, K.V., Hardisty, D.S., 2022. Modeling the impacts of diagenesis on carbonate paleoredox
516 proxies. Geochimica et Cosmochimica Acta 337, 123-139.
517 LeRoy, M.A., Gill, B.C., 2019. Evidence for the development of local anoxia during the Cambrian
518 SPICE event in eastern North America. Geobiology 17, 381-400.
519 LeRoy, M.A., Gill, B.C., Sperling, E.A., McKenzie, N.R., Park, T.-Y.S., 2021. Variable redox
520 conditions as an evolutionary driver? A multi-basin comparison of redox in the middle and later
521 Cambrian oceans (Drumian-Paibian). Palaeogeography, Palaeoclimatology, Palaeoecology 566.
522 Lu, W., Dickson, A.J., Thomas, E., Rickaby, R.E.M., Chapman, P., Lu, Z., 2020a. Refining the
523 planktic foraminiferal I/Ca proxy: Results from the Southeast Atlantic Ocean. Geochimica et
524 Cosmochimica Acta 287, 318-327.
525 Lu, Z., Hoogakker, B.A., Hillenbrand, C.-D., Zhou, X., Thomas, E., Gutchess, K.M., Lu, W., Jones,
526 L., Rickaby, R.E., 2016. Oxygen depletion recorded in upper waters of the glacial Southern Ocean.
527 Nature communications 7, 11146.
528 Lu, Z., Jenkyns, H.C., Rickaby, R.E.M., 2010. Iodine to calcium ratios in marine carbonate as a
529 paleo-redox proxy during oceanic anoxic events. Geology 38, 1107-1110.

Lu, Z., Lu, W., Rickaby, R.E., Thomas, E., 2020b. Earth History of Oxygen and the iprOxy. Cambridge University Press.
Ludvigsen, R., Westrop, S.R., 1985. Three new upper Cambrian stages for North America. Geology 13, 139-143.
Luther, G.W., Campbell, T., 1991. Iodine speciation in the water column of the Black Sea. Deep Sea Research Part A. Oceanographic Research Papers 38, S875-S882.
Mackey, J.E., Stewart, B.W., 2019. Evidence of SPICE-related anoxia on the Laurentian passive margin: Paired δ13C and trace element chemostratigraphy of the upper Conasauga Group, Central Appalachian Basin. Palaeogeography, Palaeoclimatology, Palaeoecology 528, 160-174.
Miller, J.F., Evans, K.R., Dattilo, B.F., Derby, J., Fritz, R., Longacre, S., Morgan, W., Sternbach, C., 2012. The Great American Carbonate Bank in the Miogeocline of Western Central Utah: Tectonic Influences on Sedimentation, Great American Carbonate Bank: The Geology and Economic Resources of the Cambrian—Ordovician Sauk Megasequence of Laurentia. American Association of Petroleum Geologists, p. 0.
Mount, J.F., Bergk, K.J., 1998. Depositional Sequence Stratigraphy of Lower Cambrian Grand Cycles, Southern Great Basin, U.S.A. International Geology Review 40, 55-77.
Osleger, D., Read, J.F., 1991. Relation of eustasy to stacking patterns of meter-scale carbonate cycles, Late Cambrian, USA. Journal of Sedimentary Research 61, 1225-1252.
Palmer, A.R., 1960. Trilobites of the Upper Cambrian Dunderberg shale, Eureka district, Nevada, Professional Paper, - ed.
Palmer, A.R., 1984. The biomere problem; evolution of an idea. Journal of Paleontology 58, 599-611.
Palmer, A.R., Holland, C., 1971. The Cambrian of the Great Basin and adjacent areas, western United States. Cambrian of the New World 1, 1-78.
Peng, S., 1992. Upper Cambrian biostratigraphy and trilobite faunas of the Cili - Taoyuan area，northwestern Hunan，China.
Peng, S., Babcock, L., Robison, R., Lin, H., Rees, M., Saltzman, M., 2004. Global Standard Stratotype-section and Point (GSSP) of the Furongian Series and Paibian Stage (Cambrian). Lethaia 37, 365-379.
Peng, S., Babcock, L.E., Zuo, J., Lin, H., Zhu, X., Yang, X., Robison, R.A., Qi, Y., Bagnoli, G., Chen, Y.a., 2009. The global boundary stratotype section and point (GSSP) of the Guzhangian Stage (Cambrian) in the Wuling Mountains, northwestern Hunan, China. Episodes Journal of International Geoscience 32, 41-55.
Peng, S.C., Babcock, L.E., Ahlberg, P., 2020. The Cambrian Period, Geologic Time Scale 2020, pp. 565-629.
Pohl, A., Lu, Z., Lu, W., Stockey, R.G., Elrick, M., Li, M., Desrochers, A., Shen, Y., He, R., Finnegan, S., Ridgwell, A., 2021. Vertical decoupling in Late Ordovician anoxia due to reorganization of ocean circulation. Nature Geoscience 14, 868-873.
Pohl, A., Ridgwell, A., Stockey, R.G., Thomazo, C., Keane, A., Vennin, E., Scotese, C.R., 2022. Continental configuration controls ocean oxygenation during the Phanerozoic. Nature 608, 523-527.
Pruss, S.B., Jones, D.S., Fike, D.A., Tosca, N.J., Wignall, P.B., 2019. Marine anoxia and sedimentary mercury enrichments during the Late Cambrian SPICE event in northern Scotland. Geology 47, 475-478.

Pulsipher, M.A., Schiffbauer, J.D., Jeffrey, M.J., Huntley, J.W., Fike, D.A., Shelton, K.L., 2021. A meta-analysis of the Steptoean Positive Carbon Isotope Excursion: The SPICEraq database. Earth-Science Reviews 212.
Rees, M., 1986. A fault-controlled trough through a carbonate platform: the Middle Cambrian House Range embayment. Geological Society of America Bulletin 97, 1054-1069.
Ridgwell, A., Hargreaves, J.C., Edwards, N.R., Annan, J.D., Lenton, T.M., Marsh, R., Yool, A., Watson, A., 2007. Marine geochemical data assimilation in an efficient Earth System Model of global biogeochemical cycling. Biogeosciences 4, 87-104.
Saltzman, M.R., Cowan, C.A., Runkel, A.C., Runnegar, B., Stewart, M.C., Palmer, A.R., 2004. The Late Cambrian SPICE (δ13C) event and the Sauk II-Sauk III regression: new evidence from Laurentian basins in Utah, Iowa, and Newfoundland. Journal of Sedimentary Research 74, 366-377.
Saltzman, M.R., Ripperdan, R.L., Brasier, M., Lohmann, K.C., Robison, R.A., Chang, W., Peng, S., Ergaliev, E., Runnegar, B., 2000. A global carbon isotope excursion (SPICE) during the Late Cambrian: relation to trilobite extinctions, organic-matter burial and sea level. Palaeogeography, Palaeoclimatology, Palaeoecology 162, 211-223.
Saltzman, M.R., Runnegar, B., Lohmann, K.C., 1998. Carbon isotope stratigraphy of Upper Cambrian (Steptoean Stage) sequences of the eastern Great Basin: Record of a global oceanographic event. Geological Society of America Bulletin 110, 285-297.
Saltzman, M.R., Young, S.A., Kump, L.R., Gill, B.C., Lyons, T.W., Runnegar, B., 2011. Pulse of atmospheric oxygen during the late Cambrian. Proc Natl Acad Sci U S A 108, 3876-3881.
Scotese, C.R., Wright, N., 2018. PALEOMAP paleodigital elevation models (PaleoDEMS) for the Phanerozoic. Paleomap Proj.
Servais, T., Perrier, V., Danelian, T., Klug, C., Martin, R., Munnecke, A., Nowak, H., Nützel, A., Vandenbroucke, T.R.A., Williams, M., Rasmussen, C.M.Ø., 2016. The onset of the 'Ordovician Plankton Revolution' in the late Cambrian. Palaeogeography, Palaeoclimatology, Palaeoecology 458, 12-28.
Sperling, E.A., Wolock, C.J., Morgan, A.S., Gill, B.C., Kunzmann, M., Halverson, G.P., Macdonald, F.A., Knoll, A.H., Johnston, D.T., 2015. Statistical analysis of iron geochemical data suggests limited late Proterozoic oxygenation. Nature 523, 451.
Stockey, R.G., Pohl, A., Ridgwell, A., Finnegan, S., Sperling, E.A., 2021. Decreasing Phanerozoic extinction intensity as a consequence of Earth surface oxygenation and metazoan ecophysiology. Proc Natl Acad Sci U S A 118.
Taufani, L., 2012. Detrital Carbonates in a Sequence Stratigraphic Framework: An example from the Furongian Slope Environment in the Hot Creek Range of Central Nevada, Geoscience, p. 96.
Taylor, M.E., Cook, H.E., Melnikova, L., 1991. Biofacies evidence for Late Cambrian low-paleolatitude oceans, western United State and central Asia, Journal Name: AAPG Bulletin (American Association of Petroleum Geologists); (United States); Journal Volume: 75:2; Conference: American Association of Petroleum Geologists (AAPG)/Society of Economics, Paleontolgists, and Mineralogists (SEPM)/Society of Exploration Geophysicists (SEG)/Society of Professional Well Log Analysts (SPWLA) Pacific Section annual meeting, Bakersfield, CA (United States), 6-8 Mar 1991, United States, p. Medium: X; Size: Pages: 383.
Tostevin, R., Mills, B.J.W., 2020. Reconciling proxy records and models of Earth's oxygenation during the Neoproterozoic and Palaeozoic. Interface Focus 10.

Wallace, M.W., Shuster, A., Greig, A., Planavsky, N.J., Reed, C.P., 2017. Oxygenation history of the Neoproterozoic to early Phanerozoic and the rise of land plants. Earth and Planetary Science Letters 466, 12-19.
Widiarti, R., 2011. Lateral variability of facies and cycles in the Furongian (Late Cambrian) Carbonate Platform: An example from the Big Horse Member of the Orr Formation in western Utah, USA, Geoscience. University of Nevada, Las Vegas, p. 66.
Zeiza, A.D., 2010. Tectonically Controlled Autocyclicity in the Furongian (Late Cambrian) Carbonate Platform, Central Nevada and Western Utah, USA, Geoscience. University of Nevada, Las Vegas, p. 91.
Zhang, L., Algeo, T.J., Zhao, L., Chen, Z.-Q., Zhang, Z., Li, C., 2022. Linkage of the late Cambrian microbe-metazoan transition (MMT) to shallow-marine oxygenation during the SPICE event. Global and Planetary Change 213.
Zhao, Z., Pang, X., Zou, C., Dickson, A.J., Basu, A., Guo, Z., Pan, S., Nielsen, A.T., Schovsbo, N.H., Jing, Z., Dahl, T.W., 2023. Dynamic oceanic redox conditions across the late Cambrian SPICE event constrained by molybdenum and uranium isotopes. Earth and Planetary Science Letters 604.
Zhou, X., Jenkyns, H.C., Owens, J.D., Junium, C.K., Zheng, X.-Y., Sageman, B.B., Hardisty, D.S., Lyons, T.W., Ridgwell, A., Lu, Z., 2015. Upper ocean oxygenation dynamics from I/Ca ratios during the Cenomanian-Turonian OAE 2. Paleoceanography 30, 510-526.
Zhu, M.-Y., Babcock, L.E., Peng, S.-C., 2006. Advances in Cambrian stratigraphy and paleontology: Integrating correlation techniques, paleobiology, taphonomy and paleoenvironmental reconstruction. Palaeoworld 15, 217-222.
Zhu, M.-Y., Zhang, J.-M., Li, G.-X., Yang, A.-H., 2004. Evolution of C isotopes in the Cambrian of China: implications for Cambrian subdivision and trilobite mass extinctions. Geobios 37, 287-301.
Zuo, J., Peng, S., Qi, Y., Zhu, X., Bagnoli, G., Fang, H., 2018. Carbon-Isotope Excursions Recorded in the Cambrian System, South China: Implications for Mass Extinctions and Sea-Level Fluctuations. Journal of Earth Science 29, 479-491.